INORGANIC CHEMISTRY FRONTIERS

RESEARCH ARTICLE

View Article Online
View Journal | View Issue

Cite this: *Inorg. Chem. Front.*, 2024, **11**, 3367

Exploration of antimony(III) oxyhalides *via* single-site substitution in quest of large birefringence†

Chenhui Hu,‡[a,b] Dongdong Chu,‡[a,b] Xueling Hou,[a,b] Feng Zhang*[a,b] and Jian Han*[a,b]

Received 2nd March 2024,
Accepted 27th April 2024

DOI: 10.1039/d4qi00564c

rsc.li/frontiers-inorganic

Birefringent crystals play a crucial role in the laser polarization of modern laser technologies. As a marvelous branch of optical materials, oxyhalides are attracting extensive interest for their suitable structures and diverse properties. Metal cations with lone pairs have proven advantageous for enhancing birefringence and extending the range of transmission. In this study, we comprehensively investigated the antimony(III) oxyhalide system, Sb–O–X. Specifically, we systematically examined the impact of single-site substitution within a series of compounds, including SbOCl, Sb_2OCl_4, Sb_3O_4F, Sb_3O_4I, Sb_3O_4Cl, $Sb_8O_{11}Cl_2$, and $Sb_8O_{11}Br_2$. The substitution of halogens led to significant alterations in the crystal structures, ranging from 0D isolated units to 2D layers, which are favorable for generating birefringences greater than 0.1. These findings underscore the potential of antimony oxyhalides for achieving the balance between birefringence and bandgap, and affirm the viability of single-site substitution as an effective strategy for discovering birefringent materials.

Introduction

The polarization of light, as an extraordinary natural phenomenon, has yielded numerous discoveries and a wide array of applications. Crystals with great birefringence have played a pivotal role in both research and engineering domains for manipulating the polarization of light, encompassing applications in polarimetry, optical fibers, and the laser industry. The discovery of the new birefringent materials system has attracted considerable academic and commercial attention. As nonlinear optical (NLO) materials continue to advance rapidly, there is a pressing need for birefringent materials due to their essential technological attributes in the manipulation of light polarization.[1–7] Several birefringent materials, including MgF_2,[8] α-BaB_2O_4,[9,10] $CaCO_3$,[11] TiO_2,[12] and YVO_4 crystals,[13] have been harnessed for applications spanning from the deep-ultraviolet (DUV) to the near-infrared (NIR) regions. With the increased demand for birefringent materials, materials and systems with large birefringence still deserve to be discovered. Consequently, scientists continually explore birefringent functional units and structures to achieve great birefringence.[14,15]

It is widely recognized that birefringence is intricately linked to the anisotropic polarizability of material structure. To harness this characteristic, researchers have often selected π-conjugated planar groups, such as $(NO_3)^-$, $(CO_3)^{2-}$, $(BO_3)^{3-}$, $(B_3O_6)^{3-}$, $(C_3N_6)^{6-}$, $(C_4O_4)^{2-}$, and $(C_3N_3O_3)^{3-}$, as ideal motifs for designing birefringent materials due to their notably large anisotropic linear polarizability.[16–37] In contrast to their purely oxidized tetrahedral counterparts, non-π-conjugated heterotetrahedra, such as $[BO_xF_{4-x}](x = 0–4)$, $[SO_3F]$, $[PO_xF_{4-x}](x = 2, 3)$, $[PO_xS_{4-x}](x = 0–4)$, and $[SiO_xN_{4-x}](x = 0–4)$, have been reported to exhibit an increased birefringence.[38–47] These findings suggest that the exploration of birefringent materials can be broadened to a much broader horizon by finding new birefringent units.

In recent years, there has been a significant surge of interest in oxyhalides due to their applications in energy, environmental processes, ion conductivity, and photocatalytic activities.[48–50] Oxyhalides are also emerging as promising candidates for the IR region, primarily because of their

[a]*Research Center for Crystal Materials; State Key Laboratory of Functional Materials and Devices for Special Environmental Conditions; Xinjiang Key Laboratory of Functional Crystal Materials; Xinjiang Technical Institute of Physics and Chemistry, CAS, 40-1 South Beijing Road, Urumqi 830011, China.*
E-mail: zhangfeng@ms.xjb.ac.cn, hanjian@ms.xjb.ac.cn
[b]*Center of Materials Science and Optoelectronics Engineering, University of Chinese Academy of Sciences, Beijing 100049, China*

†Electronic supplementary information (ESI) available: Experimental section, powder XRD, DSC and TG data, IR and UV-vis-NIR spectra, energy dispersive X-ray spectroscopy, the detailed theoretical calculations, and important bond distances of the compounds. CCDC 2184486 and 2184488. For ESI and crystallographic data in CIF or other electronic format see DOI: https://doi.org/10.1039/d4qi00564c

‡These authors contributed equally to this work.

exceptional resistance to laser-induced damage (LD).[51–57] Compared to pure metal oxides and halides, oxyhalides exhibit a more favorable balance between bandgap and birefringence. The incorporation of halogens leads to structural distortions and increases polarizability anisotropy. Furthermore, the introduction of cations with lone pairs, such as Sb^{3+}, Bi^{3+}, Pb^{2+}, and Sn^{2+}, proves advantageous for extending the IR cutoff edge and achieving greater birefringence when compared to the spherical-shaped alkali and alkali earth metal ions.[58–69] A recent example of this phenomenon is the about 60 times enhancement of the birefringence in α-$NaSb_3P_2O_{10}$ over $K_3SbP_2O_9$. This remarkable enhancement is attributed to the presence of the Sb^{3+} cations with stereochemically active lone pair in α-$NaSb_3P_2O_{10}$, while the Sb^{5+} cations in $K_3SbP_2O_9$ carry no lone pair.[64] These findings underline the significant contribution of Sb^{3+} cations with lone pairs to birefringence. As a result, oxyhalides with variable antimony(III)-centered polyhedra would open the door to a multitude of fascinating structural possibilities.

While the incorporation of [Sb–O–X] (X = halide) polyhedra has been explored as a means to enhance birefringence in crystals, it is important to note that not all crystals containing such polyhedra exhibit exceptional birefringence. This is because the extent of birefringence enhancement is closely linked to the specific arrangement of these polyhedra. Therefore, a practical approach to exploring superior crystals is to use known structural templates as guidance. In the prototype structure templates, the contributions of birefringence-active polyhedra to the overall birefringence have been optimized. For instance, zero-dimensional (0D) $(B_3O_6)^{3-}$ units in α-BBO and two-dimensional (2D) $[Be_2BO_3F_2]_\infty$ layered frameworks in KBBF are known to represent the optimal templates for generating significant birefringence. Following this guidance, we proposed to use isolated [Sb–O–X] polyhedra with larger anisotropy to resemble the $(B_3O_6)^{3-}$ units and to use [Sb–O–X] layers to resemble the $[Be_2BO_3F_2]_\infty$ layers in quest of large birefringence. In these systems, the halogen ions and the cations with lone pairs usually act like "chemical scissors", leading to the formation of low-dimensional frameworks that are favorable for generating large birefringence.[69]

In light of the considerations mentioned above, the antimony(III) oxyhalide, Sb_2OCl_4, was successfully designed and synthesized through the slow evaporation of a solution under open ambient conditions. Significantly, this compound features isolated $[Sb_4O_2Cl_8]$ units and demonstrates substantial birefringence. Notably, this finding underscores the significant contribution of arrangement with the isolated strong anisotropic [Sb–O–Cl] polyhedron. Furthermore, in the context of the antimony–oxyhalide system, several compounds have been selected and investigated, including layered structures: Sb_3O_4F, Sb_3O_4I, Sb_3O_4Cl, $Sb_8O_{11}Cl_2$, and $Sb_8O_{11}Br_2$,[70–77] and their birefringence all exhibit greater than 0.1.

In summary, this research encompassed the synthesis, UV-vis-NIR diffuse reflectance spectroscopy, IR spectroscopy, and thermal stability analysis of the compounds. First-principles calculations were also conducted for these compounds to elucidate the relationship between their electronic structure and optical properties.

Results and discussion

Single-site substitution of the anions

Single-site substitution stands as an effective strategy in the synthesis of the crystals. In this approach, a single cation or anion within the crystal structure is replaced by another ion from the same group in the periodic table, typically when there is similarity in cation radii. This substitution can involve ions like NH_4^+, K^+, Rb^+, and Cs^+, leading to the creation of a wide range of exceptional materials. Anions are also amenable to single-site substitution, especially halogens. Nevertheless, the impact of such substitution on birefringence, such as when Cl atoms are replaced by the larger and more polarizable Br atoms, remains a subject of ongoing investigation. Inspired by the successful replacement of oxygen atoms in borate compounds with fluorine atoms to produce superior fluorooxoborates, we considered the replacement of the O(Cl) atom in SbOCl with the Cl(O) atom. This simple crystal served as a foundational template to explore the development of materials. As Fig. 1 shows, based on the foundational compound SbOCl, we designed and researched these antimony(III) oxyhalides: Sb_2OCl_4, Sb_3O_4F, Sb_3O_4I, Sb_3O_4Cl, $Sb_8O_{11}Cl_2$, and $Sb_8O_{11}Br_2$, primarily through the substitution of single-site anions.

Structure description

All of the SbOCl, Sb_2OCl_4, and Sb_3O_4F compounds crystallize in space group $P2_1/c$. On the other hand, both $Sb_8O_{11}Cl_2$ and

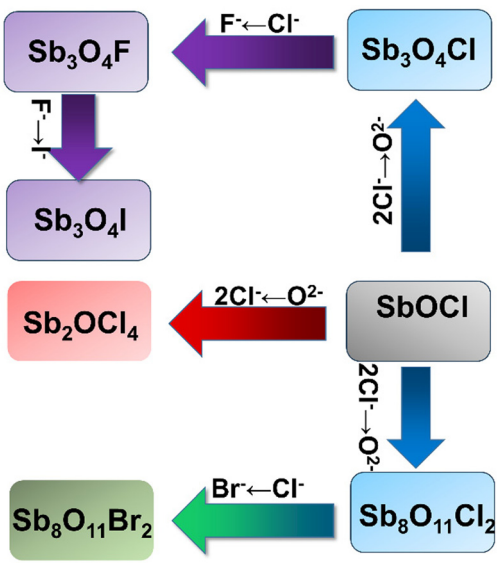

Fig. 1 Schematic illustration of the relationship between the template compound SbOCl and six antimony(III) oxyhalides, Sb_2OCl_4, Sb_3O_4F, Sb_3O_4I, Sb_3O_4Cl, $Sb_8O_{11}Cl_2$, and $Sb_8O_{11}Br_2$, explored *via* single-site substitution.

$Sb_8O_{11}Br_2$ crystallize in space group $P\bar{1}$. However, Sb_3O_4Cl and Sb_3O_4I exhibit different space groups, specifically $P2/c$ and $Pna2_1$, respectively. It is worth noting that the bond lengths for the covalent Sb–Cl bonds in $SbCl_3$ range from 2.340 to 2.368 Å, while the Sb–Br bond lengths in α-$SbBr_3$ and β-$SbBr_3$ range from 2.459 to 2.542 Å. In the case of $Sb_8O_{11}Cl_2$, the shortest Sb–Cl bond length is 2.95 Å, and in $Sb_8O_{11}Br_2$, it is 3.14 Å. These relatively longer bond lengths, along with the small bond valence sum for the halide ions, suggest an ionic character of the Sb–X bonds in $Sb_8O_{11}Cl_2$ and $Sb_8O_{11}Br_2$.

The structures of four typical antimony oxyhalide compounds are described in Fig. 2a–d. As shown in Fig. 2a, each asymmetric unit of SbOCl comprises three Sb atoms, three O atoms, and three Cl atoms. The structure is composed of $(SbO_4)^{5-}$ and $(SbO_2Cl)^{2-}$ groups. $(Sb_6O_7Cl_3)^{+}$ units are interconnected *via* oxygen atoms to form a channel structure. Chlorine ions are inserted into the channels to balance the charges, ultimately creating a three-dimensional structure.

As shown in Fig. 2b, each asymmetric unit of Sb_2OCl_4 consists of two Sb atoms, one O atom, and three Cl atoms. The crystal structure is built from $(SbOCl_3)^{2-}$ and $(SbO_2Cl_2)^{3-}$ groups. Isolated $[Sb_4O_2Cl_8]$ units are interconnected to form a three-dimensional structure. As shown in Fig. 2c, each asymmetric unit of Sb_3O_4Cl includes two Sb atoms, one O atom, and two Cl atoms. The crystal structure forms a two-dimensional (2D) $[Sb_3O_4]_\infty$ layered framework, composed of $(SbO_4)^{5-}$ and $(SbO_3)^{3-}$ groups. Chlorine anions occupy the spaces between the layers to maintain charge balance. As shown in Fig. 2d, each asymmetric unit of $Sb_8O_{11}Cl_2$ includes sixteen Sb atoms, twenty-two O atoms, and four Cl atoms. The crystal structure forms a 2D $[Sb_8O_{11}]_\infty$ layered framework, composed of $(SbO_4)^{5-}$ and $(SbO_3)^{3-}$ groups. Similar to Sb_3O_4Cl, chlorine anions are positioned between the layers to maintain charge balance.

Powder X-ray diffraction

The experimental X-ray Diffraction (XRD) curves closely match the theoretical ones for five compounds, as depicted in Fig. S1.† These results not only affirm the phase purity of the materials but also confirm the presence of each constituent element within the crystals, thereby substantiating the structural validity.

Optical properties

In Fig. S2,† the IR absorption spectra of SbOCl, Sb_2OCl_4, Sb_3O_4I, $Sb_8O_{11}Cl_2$, and $Sb_8O_{11}Br_2$ reveal that the regions without obvious absorption for these powders fall within the range of 4000–725, 703, 705, 783, and 691 cm^{-1}, respectively. The IR absorption is induced by the Sb–O stretching vibrations. Fig. S3† illustrates the UV-vis-NIR diffuse-reflectance spectra for these compounds, which provide insight into their bandgaps. The bandgaps obtained by conversion are 4.02 eV for SbOCl, 3.83 eV for Sb_2OCl_4, 3.20 eV for Sb_3O_4I, 3.59 eV for $Sb_8O_{11}Cl_2$, and 3.47 eV for $Sb_8O_{11}Br_2$. The compounds with a relatively large bandgap, which may have high laser damage thresholds, are suitable for practical applications. The analysis of element type by energy dispersive spectroscopy (EDS) confirms the existence of the Sb, O, and Cl elements of Sb_2OCl_4 (Fig. S4 in the ESI†).

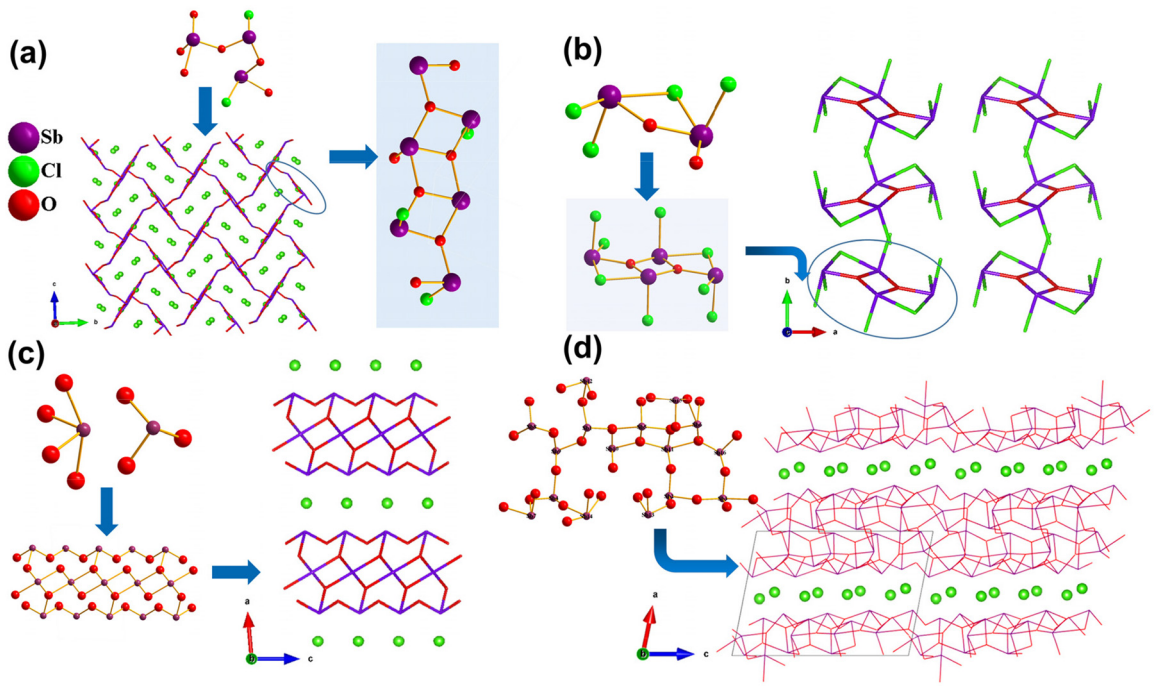

Fig. 2 Crystals structure information about compounds studied in this work. (a) The structure of SbOCl along the *a* axis; (b) the structure of Sb_2OCl_4 along the *c* axis; (c) the structure of Sb_3O_4Cl along the *b* axis; (d) the structure of $Sb_8O_{11}Cl_2$ along the *c* axis.

Thermal stability

The thermal behaviors of SbOCl, Sb_2OCl_4, Sb_3O_4I, $Sb_8O_{11}Cl_2$, and $Sb_8O_{11}Br_2$ are depicted in Fig. S5.† SbOCl, Sb_2OCl_4, and Sb_3O_4I exhibit stability up to approximately 200 °C, while $Sb_8O_{11}Cl_2$ and $Sb_8O_{11}Br_2$ remain stable up to approximately 500 °C. Differential scanning calorimetry (DSC) curves reveal several endothermic peaks for SbOCl, Sb_2OCl_4, Sb_3O_4I, $Sb_8O_{11}Cl_2$, and $Sb_8O_{11}Br_2$, which implies that they break down. During the heating process, an evident weight loss is observed, and an endothermic peak emerges at around 220 °C, signifying a decomposition reaction in SbOCl. Upon further heating to 300 °C, the formation of liquid substances with a low melting point is evident in the product of the decomposition reaction. Simultaneously, an analysis of the melted samples indicates the presence of $Sb_4O_5Cl_2$ as a significant component, along with amorphous $SbCl_3$. This suggests that the reaction can be described as follows:

$$5SbOCl \rightarrow Sb_4O_5Cl_2 + SbCl_3$$

Theoretical calculations

The electronic structure and optical properties of SbOCl, Sb_2OCl_4, Sb_3O_4F, Sb_3O_4Cl, Sb_3O_4I, $Sb_8O_{11}Cl_2$, and $Sb_8O_{11}Br_2$ were investigated using first-principles calculations. The results along the high-symmetry points of the first Brillouin zone are depicted in Fig. S6.† It is worth noting that the calculated bandgaps for these compounds are smaller than the experimental values. This outcome aligns with expectations based on the density functional theory (DFT) method, which typically underestimates bandgap. This discrepancy is primarily attributed to inaccuracies in calculating the exchange–correlation energy. To address this issue, the Perdew–Burke–Ernzerhof (PBE0) hybrid functional was employed to obtain more accurate bandgap values. The difference between the bandgap value calculated by generalized gradient approximation (GGA) and the one by PBE0 (or the experimental value) was used as an adjustment factor to calculate the optical properties of these compounds. This approach helps refine the accuracy of the calculated optical properties, compensating for the initial underestimation of bandgaps by the DFT method.

Indeed, the behavior of valence electrons is widely recognized to have a crucial influence on the optical properties of a compound, particularly in the context of band structures near the Fermi level. Therefore, a more comprehensive examination of the electronic structure within this energy range was conducted to gain insights into its impact on bandgap and optical properties. As depicted in Fig. S6,† the electronic structures, density of states (DOS), and partial density of states (PDOS) are presented for the Sb, O, and X (X = halogens) orbitals in the seven compounds. This detailed analysis provides a deeper understanding of the distribution of electronic states and the contribution of specific atomic orbitals to the electronic structure, which, in turn, influences the optical properties and bandgaps of these materials.

Origin of the differences between the birefringence of compounds

The relationship between crystal structures and their corresponding microscopic groups is undeniably intertwined with the optical properties of materials. Factors such as the arrangement of anionic frameworks and the various combinations of metal cation polyhedra significantly influence properties like birefringence. To evaluate the birefringence, a polarizing microscope method was employed to test the difference in refractive index utilizing the natural growth plane. In Fig. 3a, the original interference color of the selected Sb_2OCl_4 crystal is shown under orthogonally polarized light. The crystal thickness is approximately 9.82 μm (Fig. 3b). As shown in Fig. 3c, the drum wheel of the Berek compensator was rotated to cause the crystal achieve extinction, and the optical path differences at a wavelength of 546 nm amount to 1.45 μm according to the tables of the Berek compensator specification. By applying the relevant formula, the refractive index differences were calculated to be 0.148. The experimental birefringences of Sb_2OCl_4 crystals were found to be greater than 0.148 at 546 nm, thus validating the calculated value.

Table 1 reveals that the Sb_2OCl_4 compound exhibits a birefringence of 0.175 at 546 nm, which is about 14.6 times that of MgF_2. The improvement of the crystal structure of SbOCl through single-site substitution, along with well-considered halogen replacements, results in the creation of enhanced compounds, namely Sb_2OCl_4, which exhibits an even more significant increase at 2.6 times the birefringence of the original compound. This birefringence value is on par with other recently reported materials, such as $Sn_2B_5O_9Cl$ (0.168 at 546 nm), Sn_2PO_4Cl (0.181 at 546 nm), and SnF_2 (0.177 at 546 nm). These findings highlight the promising optical pro-

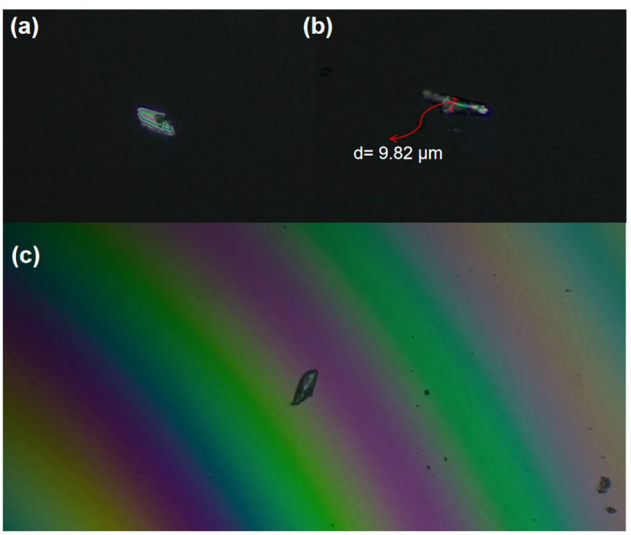

Fig. 3 Birefringence measurements for the Sb_2OCl_4 crystals. (a) Original interference color of the Sb_2OCl_4 crystal under orthogonally polarized light. (b) The thickness view of Sb_2OCl_4 crystal. (c) Extinction of the measurement of refractive index difference.

Table 1 The bandgap and birefringence of selected antimony halides, antimony oxyhalides, and commercial birefringent crystals[2]

Compound	Band gap (eV)	Birefringence
SbF_3	4.30	0.104@546 nm[a]
Sb_3O_4F	3.82[a]	0.192@546 nm[a]
SbOCl	4.02	0.067@546 nm[a]
Sb_2OCl_4	3.83	0.175@546 nm[a]
Sb_3O_4Cl	3.69[a]	0.107@546 nm[a]
$SbCl_3$	4.51[a]	0.173@546 nm[a]
$Sb_8O_{11}Cl_2$	3.59	0.129@546 nm[a]
$Sb_8O_{11}Br_2$	3.47	0.110@546 nm[a]
Sb_3O_4I	3.20	0.284@546 nm[a]
MgF_2	11.27	0.014@193 nm
α-BBO	6.56	0.122@532 nm
$CaCO_3$	3.54	0.171@633 nm
TiO_2	3.10	0.256@1530 nm
YVO_4	3.10	0.225@633 nm

[a] Calculated value.

perties of Sb_2OCl_4 in comparison to other relevant compounds.

It is well-known that different structures and compositions often lead to distinct material performances. In explaining the differences in birefringence between SbF_3 and Sb_3O_4F, a comparative analysis of their structures and metal polyhedra is essential. To begin with, the Sb_3O_4F crystal possesses a monoclinic crystal system with lower symmetry than SbF_3. Additionally, the introduction of halogen atoms with stereochemically active lone pairs can enhance optical anisotropy. One key distinguishing factor is the coordination of metal polyhedra. The $(SbO_3F)^{4-}$ polyhedra found in Sb_3O_4F have more oxygen ligands and exhibit a pronounced asymmetric coordination of metal polyhedra compared to the $[SbF_3]$ polyhedra. The $(SbO_3F)^{4-}$ polyhedron also demonstrates a more typical asymmetric structure of metal polyhedra due to the presence of lone pairs. These differences in structure and coordination contribute to the varying birefringence properties observed in Sb_3O_4F compared to SbF_3.

The arrangement of polyhedra with lone pairs profoundly impacts optical anisotropy. Using SbOCl as a template structure, structural modifications were made to create compounds with enhanced birefringence. In the case of Sb_2OCl_4, two chlorine (Cl) atoms were replaced with one oxygen (O) atom, leading to a significant gain in birefringence. Sb_2OCl_4 exhibits isolated $[Sb_4O_2Cl_8]$ units, transforming the initially unfavorable pore structure into 0D birefringent active units reminiscent of α-BBO. On the other hand, by replacing one oxygen atom with two chlorine atoms, Sb_3O_4Cl was obtained. This compound features a distinct laminar structure, similar to KBBF, which contributes to the gain in birefringence. This structural modification, compared to SbOCl, leads to a significant increase in birefringence, emphasizing the role of structural transformations in enhancing optical properties.

In alkali and alkaline-earth metal borates, it is noteworthy that many compounds with chlorine (Cl) are isostructural with their bromine (Br) counterparts. However, the interesting observation is that there is often very little difference in birefringence between the chloride and bromide variants of these compounds. Examples of such compounds include $K_3B_6O_{10}X$ (X = Cl, Br), $Li_3B_8O_{13}X$ (X = Cl, Br), and $Ba_3P_3O_{10}X$ (X = Cl, Br).[78–84] This suggests that the alkali and alkaline-earth metal polyhedra have a relatively small influence on birefringence.[94] Thus, the change in halogen from Cl to Br does not significantly affect birefringence in these cases. However, the situation is different when the halogens are changed from chlorine to iodine. In these cases, there is a noticeable increase in birefringence. Examples of compounds exhibiting this trend include Pb_2BO_3X (X = Cl, Br, I), SnB_3O_7X (X = Cl, Br), SnB_5O_9X (X = Cl, Br), Sn_2PO_4X (X = F, Cl, Br, I), and $PbSn(PO_4)X$ (X = Cl, Br, I).[85–93] This indicates that the change in halogen from Cl to Br or I has a more pronounced effect on birefringence in these compounds, leading to increased optical anisotropy.

The introduction of halogens has a different effect on the birefringence of compounds containing cations with lone pairs, and this effect can be attributed to several factors. In the case of Sb_3O_4Cl and Sb_3O_4I, there is a gradual increase in birefringence from the chloride to the bromide compound. This trend is primarily related to the electronegativity of the halogen ions. This decrease in electronegativity strengthens the interaction between antimony and the halogen ions. As a result, the stereochemical activity of lone pairs in the [Sb–O–X] polyhedra increases gradually. This enhanced stereochemical activity of lone pairs is responsible for the observed increase in birefringence. Similar phenomena can be observed in other compounds, where changes in the halogen type (Cl^- to Br^-) lead to an increase in birefringence. The combination of factors, including electronegativity and the arrangement of basic building units, contributes to the gradual increase in birefringence in compounds like Sb_3O_4X (X = Cl, I).

The absence of a noticeable increase in birefringence from $Sb_8O_{11}Cl_2$ to $Sb_8O_{11}Br_2$, despite the different polarization rates of chlorine and bromine, can be explained by examining the specific contributions of the [Sb–O–X] polyhedra and the Sb–Cl/Br bonds. In this case, the [Sb–O–X] polyhedra have comparatively weak Sb–Cl/Br bonds, and the differences in polarization rates between Cl^- and Br^- in these bonds have a limited impact on the overall birefringence. By contrast, the primary source of birefringence in these compounds comes from the [Sb–O] polyhedra. The larger atomic radius of bromine compared to chlorine does affect the density of the birefringent effective primitive, which can, in turn, lead to a smaller birefringence for $Sb_8O_{11}Br_2$ than for $Sb_8O_{11}Cl_2$. This effect is particularly relevant when considering the structural arrangement and contributions of the [Sb–O–X] polyhedra. This same phenomenon can be observed in Sb_3O_4X (X = F, Cl), where Sb_3O_4Cl has a smaller birefringence than Sb_3O_4F through Cl to F with a larger polarization rate. The primary contributing factor in these cases is the [Sb–O–X] polyhedra, while the Sb–Cl bond, due to its excessive length, does not significantly impact birefringence.

Theoretical analysis

To further understand the origin of the large birefringence in these compounds resulting from electronic transitions, several key electronic properties are analyzed, including the DOS, PDOS, band structure, and the negative crystal orbital Hamilton population (COHP). The analysis reveals that the linear response primarily occurs in the bottom region of the conduction bands (CBs). This is because large orbital hybridization interactions, specifically between O-2p orbitals and Sb-5s and 5p orbitals, are induced by the stereochemical activity of lone pairs and the anisotropic distribution of electronic density. In the top region of the valence bands (VBs), the states are mainly occupied by the 5s and 5p states of Sb, the 2p states of O, and the p states of the halogen anions. Furthermore, antibonding states between Sb and O are also occupied in this region. The bottom region of the conduction bands (CBs) is primarily occupied by the 5p states of Sb, which play a significant role below the Fermi level. The anisotropy of the polyhedra depends on the strength of the stereochemical activity. Importantly, the interplay between the Sb-5s state and the p states of the anions, with sufficient energy, results in a filled antibonding Sb-s and p state of the anion combination, which is clearly shown in Fig. 4. In addition, when examining the PDOS and COHP, it becomes evident that there is a bonding interaction between the p orbitals of the anions and the 5s and 5p orbitals of the cations near the Fermi level. This interaction also allows for the coupling of the s and p states of the cation, leading to a spatially uneven electron density on antimony, which is responsible for the stereochemical activity. In essence, polyhedra with significant stereochemical activity are crucial for generating large anisotropies in the microstructure. When combined with favorable structural patterns, these polyhedra contribute to the formation of compounds with substantial birefringence.

Our previous work sheds light on an interesting trend among oxyhalides based on the choice of cation.[51] Oxyhalides with alkaline earth metals tend to exhibit large bandgaps but generally have small birefringence. On the other hand, oxyhalides containing bismuth tend to display moderate birefringence but have a relatively small bandgap. As shown in Fig. 5, oxyhalides in the antimony family strike a balance between birefringence and bandgaps. Sb_2OCl_4 offers a promising combination of substantial birefringence and ease of synthesis at low temperatures. This suggests that antimony oxyhalides have the potential to be excellent candidates for birefringent materials, making them an attractive option for various applications.

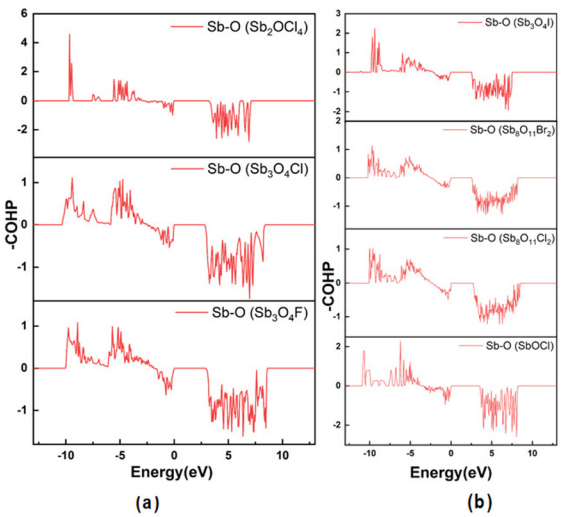

Fig. 4 COHP information on (a) Sb_2OCl_4, Sb_3O_4Cl, and Sb_3O_4F, (b) Sb_3O_4I, $Sb_8O_{11}Br_2$, $Sb_8O_{11}Cl_2$, and SbOCl.

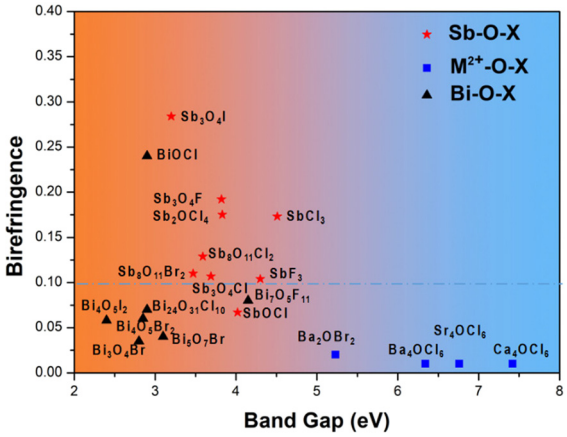

Fig. 5 Comparison between the compounds synthesized in this work (☆) and the reported ones in terms of birefringence and bandgap.

Conclusions

Using the SbOCl compound as a template, we researched six antimony(III) oxyhalides, including Sb_2OCl_4, Sb_3O_4F, Sb_3O_4I, Sb_3O_4Cl, $Sb_8O_{11}Cl_2$, and $Sb_8O_{11}Br_2$, *via* single-site substitution. The single-site substitution leads to a diversification of structures, ranging from isolated units to layers, which are favorable for generating birefringences greater than 0.1. Among these compounds, the structure of the compound Sb_2OCl_4 exhibits a remarkable birefringence value of 0.175@546 nm. By combining experimental measurements and first-principles calculations, we clarified that these antimony(III) oxyhalides exhibit substantial birefringence and relatively large bandgaps (ranging from 3 to 4.5 eV), which implies that the system is balanced between birefringence and bandgap. These compounds were designed by using structural templates and single-site substitution, serving as a successful strategy for the exploration and design of structure-driven functional materials with significant birefringence.

Data availability

All of the related experimental and computational data are provided in the ESI.†

Author contributions

C. H. H. and J. H. designed the research study; C. H. H. synthesized the compound; C. H. H. and X. L. H. performed the experiments. D. D. C. and F. Z. performed the optical theoretical calculations. All authors wrote and revised the manuscript. All the authors contributed to the final manuscript preparation.

Conflicts of interest

The authors declare no competing financial interests.

Acknowledgements

This work was financially supported by the Key Research and Development Program of Xinjiang (2022B01023-3), Tianshan Talent Training Program (2023TSYCLJ0018), West Light Foundation of CAS (2020-XBQNXZ-002), National Natural Science Foundation of China (22335007, 22361132544, U2003131), the High-level Professional and Technical Personnel of Xinjiang Autonomous Region, and Xinjiang Major Science and Technology Project (2021A01001).

References

1 R. Appel, C. D. Dyer and J. N. Lockwood, Design of a broadband UV-visible α-barium borate polarizer, *Appl. Opt.*, 2002, **41**, 2470–2480.
2 A. Tudi, S. J. Han, Z. H. Yang and S. L. Pan, Potential optical functional crystals with large birefringence: recent advances and future prospects, *Coord. Chem. Rev.*, 2022, **459**, 214380.
3 F. F. Zhang, X. L. Chen, M. Zhang, W. Q. Jin, S. J. Han, Z. H. Yang and S. L. Pan, An excellent deep-ultraviolet birefringent material based on $[BO_2]_\infty$ infinite chains, *Light: Sci. Appl.*, 2022, **11**, 252.
4 J. Zhang, C. F. Wu, H. S. Shi, C. W. Xie, Z. H. Yang and S. L. Pan, An interlinked prediction-experiment paradigm discovering deep-ultraviolet fluorooxoborates with desired optical nonlinearity and birefringence, *Matter*, 2023, **6**, 1188–1202.
5 D. Wang, Z. Wang, Z. Zhang, Y. Yue, D. Li and C. Maple, Effects of polarization on four-beam laser interference lithography, *Appl. Phys. Lett.*, 2013, **102**, 081903.
6 C. M. Huang, M. Mutailipu, F. F. Zhang, C. Hu, Z. H. Yang, L. Y. Wang, X. Zhou, K. R. Poeppelmeier and S. L. Pan, Pushing the limits of borates with functionalized $[BO_2]^-$ units, *Nat. Commun.*, 2021, **12**, 2597.
7 Z. Y. Xie, L. G. Sun, G. Z. Han and Z. Z. Gu, Optical switching of a birefringent photonic crystal, *Adv. Mater.*, 2008, **20**, 3601–3604.
8 M. J. Dodge, Refractive properties of magnesium fluoride, *Appl. Opt.*, 1984, **23**, 1980–1985.
9 G. Q. Zhou, J. Xu, X. D. Chen, H. Y. Zhong, S. T. Wang, K. Xu, P. Z. Deng and F. X. Gan, Growth and spectrum of a novel birefringent α-BaB_2O_4 crystal, *J. Cryst. Growth*, 1998, **191**, 517–519.
10 S. F. Wu, G. F. Wang, J. L. Xie, X. Q. Wu, Y. F. Zhang and X. Lin, Growth of large birefringent α-BBO crystal, *J. Cryst. Growth*, 2002, **245**, 84–86.
11 G. Ghosh, Dispersion-equation coefficients for the refractive index and birefringence of calcite and quartz crystals, *Opt. Commun.*, 1999, **163**, 95–102.
12 J. R. DeVore and J. R. DeVore, Refractive indices of rutile and sphalerite, *J. Opt. Soc. Am.*, 1951, **41**, 416–419.
13 L. G. DeShazer, Improved midinfrared polarizers using yttrium vanadate, *Proc. SPIE*, 2001, **4481**, 10–16.
14 W. G. Zhang, H. W. Yu, H. P. Wu and P. S. Halasyamani, Phasematching in nonlinear optical compounds: a materials perspective, *Chem. Mater.*, 2017, **29**, 2655–2668.
15 W. Q. Jin, W. Y. Zhang, A. Tudi, L. Y. Wang, X. Zhou, Z. H. Yang and S. L. Pan, Fluorine-driven enhancement of birefringence in the fluorooxosulfate: a deep evaluation from a joint experimental and computational study, *Adv. Sci.*, 2021, **8**, 2003594.
16 M. Mutailipu, K. R. Poeppelmeier and S. L. Pan, Borates: a rich source for optical materials, *Chem. Rev.*, 2020, **121**, 1130–1202.
17 Y. Yang, X. Y. Dong, Z. H. Yang and S. L. Pan, $CsBaB_9O_{15}$ with high performances as potential ultraviolet nonlinear optical material: achieved from peculiar double borate layer, *Sci. Bull.*, 2021, **66**, 2165–2169.
18 Y. Liu, Y. Shen, S. Zhao and J. Luo, Structure-property relationship in nonlinear optical materials with π-conjugated CO_3 triangles, *Coord. Chem. Rev.*, 2020, **407**, 213152.
19 Z. J. Li, W. Q. Jin, F. F. Zhang, Z. H. Yang and S. L. Pan, Exploring short-wavelength phase-matching nonlinear optical crystals by employing $KBe_2BO_3F_2$ template, *ACS Cent. Sci.*, 2022, **8**, 1557–1564.
20 Q. Jing, G. Yang, J. Hou, M. Z. Sun and H. B. Cao, Positive and negative contribution to birefringence in a family of carbonates: a born effective charges analysis, *J. Solid State Chem.*, 2016, **244**, 69–74.
21 Q. Jing, G. Yang, Z. H. Chen, X. Y. Dong and Y. J. Shi, A joint strategy to evaluate the microscopic origin of the second-harmonic generation response in nonpolar $ABCO_3F$ compounds, *Inorg. Chem.*, 2018, **57**, 1251–1258.
22 C. Wu, X. X. Jiang, X. J. Wang, Z. S. Lin, Z. P. Huang, X. F. Long, M. G. Humphrey and C. Zhang, Giant optical anisotropy in the UV-transparent 2D nonlinear optical material $Sc(IO_3)_2(NO_3)$, *Angew. Chem., Int. Ed.*, 2021, **60**, 3464–3468.
23 J. Lu, Y. K. Lian, L. Xiong, Q. R. Wu, M. Zhao, K. X. Shi, L. Chen and L. M. Wu, How to maximize birefringence and nonlinearity of π-conjugated cyanurates, *J. Am. Chem. Soc.*, 2019, **141**, 16151–16159.
24 D. H. Lin, M. Luo, C. S. Lin, F. Xu and N. Ye, $KLi(HC_3N_3O_3)\cdot 2H_2O$: Solvent-drop grinding method towards

the hydro isocyanurate nonlinear optical crystal, *J. Am. Chem. Soc.*, 2019, **141**, 3390–3394.

25 Z. J. Huang, X. Su, S. L. Pan, X. Y. Dong, S. J. Han, H. W. Yu, M. Zhang, Y. Yang, S. F. Cui and Z. H. Yang, $Sr_3B_6O_{11}F_2$: a promising polar fluoroborate with short UV absorption edge and moderate second harmonic generation response, *Scr. Mater.*, 2013, **69**, 449–452.

26 W. B. Zhang, W. Q. Jin, S. J. Han, Z. H. Yang and S. L. Pan, $Pb_3Ba_7B_7O_{20}F$: A new nonlinear optical material exhibiting large second harmonic generation response induced by its unprecedented Pb-B-O framework, *Scr. Mater.*, 2021, **194**, 113700.

27 Z. Jia, N. N. Zhang, Y. Y. Ma, L. W. Zhao, M. J. Xia and R. K. Li, Top-seeded solution growth and optical properties of deep-uv birefringent crystal $Ba_2Ca(B_3O_6)_2$, *Cryst. Growth Des.*, 2017, **17**, 558–562.

28 R. K. Li and Y. Y. Ma, Chemical engineering of a birefringent crystal transparent in the deep UV range, *CrystEngComm*, 2012, **14**, 5421–5424.

29 M. He, X. L. Chen, Y. P. Sun, J. Liu, J. T. Zhao and C. Duan, $YBa_3B_9O_{18}$: A promising scintillation crystal, *Cryst. Growth Des.*, 2007, **7**, 199–201.

30 X. Chen, B. Zhang, F. Zhang, Y. Wang, M. Zhang, Z. Yang, K. R. Poeppelmeier and S. L. Pan, Designing an excellent deep-ultraviolet birefringent material for light polarization, *J. Am. Chem. Soc.*, 2018, **140**, 16311–16319.

31 B. B. Zhang, G. Q. Shi, Z. H. Yang, F. F. Zhang and S. L. Pan, Fluorooxoborates: beryllium-free deep-ultraviolet nonlinear optical materials without layered growth, *Angew. Chem., Int. Ed.*, 2017, **56**, 3916–3919.

32 G. Q. Shi, Y. Wang, F. F. Zhang, B. B. Zhang, Z. H. Yang, X. L. Hou, S. L. Pan and K. R. Poeppelmeier, Finding the next deep-ultraviolet nonlinear optical material: $NH_4B_4O_6F$, *J. Am. Chem. Soc.*, 2017, **139**, 10645–10648.

33 M. Mutailipu, M. Zhang, B. B. Zhang, L. Y. Wang, Z. H. Yang, X. Zhou and S. L. Pan, $SrB_5O_7F_3$ functionalized with $[B_5O_9F_3]^{6-}$ chromophores: accelerating the rational design of deep-ultraviolet nonlinear optical materials, *Angew. Chem., Int. Ed.*, 2018, **57**, 6095–6099.

34 T. H. Tong, W. G. Zhang, Z. H. Yang and S. L. Pan, Series of crystals with giant optical anisotropy: a targeted strategic research, *Angew. Chem., Int. Ed.*, 2021, **60**, 1332–1338.

35 Z. H. Miao, Y. Yang, Z. L. Wei, Z. H. Yang and S. L. Pan, $Ba_2B_7O_{12}F$ with novel FBB $[B_7O_{16}F]$ and deep-ultraviolet cut-off edge, *Inorg. Chem. Front.*, 2021, **8**, 339–343.

36 M. Mutailipu, M. Zhang, Z. H. Yang and S. L. Pan, Targeting the next generation of deep-ultraviolet nonlinear optical materials: expanding from borates to borate fluorides to fluorooxoborates, *Acc. Chem. Res.*, 2019, **52**, 791–801.

37 M. Mutailipu and S. L. Pan, Emergent deep-ultraviolet nonlinear optical candidates, *Angew. Chem., Int. Ed.*, 2020, **59**, 20302–20317.

38 L. Xiong, L. Chen, J. Lu, C. Y. Pan and L. M. Wu, Monofluorophosphates: a new source of deep-ultraviolet nonlinear optical materials, *Chem. Mater.*, 2018, **30**, 7823–7830.

39 B. L. Cheng, Z. J. Li, Y. Chu, A. Tudi, M. Mutailipu, F. F. Zhang, Z. H. Yang and S. L. Pan, $(NH_4)_3B_{11}PO_{19}F_3$: A deep-UV nonlinear optical crystal with unique $[B_5PO_{10}F]_\infty$ layers, *Natl. Sci. Rev.*, 2022, **9**, nwac110.

40 H. Y. Sha, J. X. Xu, L. X. Huang, Z. Y. Xiong, Z. J. Wang, R. B. Su, H. Chao, X. M. Yang and X. F. Long, Alkali metal sulfate: A new non-π-conjugated deep-ultraviolet quasi-phase matching crystal, *Scr. Mater.*, 2022, **217**, 114764.

41 X. Y. Zhang, L. Kang, P. F. Gong, Z. S. Lin and Y. C. Wu, Nonlinear optical oxythiophosphate approaching the good balance with wide ultraviolet transparency, strong second harmonic effect and large birefringence, *Angew. Chem., Int. Ed.*, 2021, **60**, 6386–6390.

42 X. D. Zhang, L. C. Guo, B. B. Zhang, J. Yu, Y. Wang, K. Wu, H. J. Wang and M. H. Lee, From silicates to oxonitridosilicates: improving optical anisotropy for phase-matching as ultraviolet nonlinear optical materials, *Chem. Commun.*, 2021, **57**, 639–642.

43 Z. H. Yang, A. Tudi, B. H. Lei and S. L. Pan, Enhanced nonlinear optical functionality in birefringence and refractive index dispersion of the deep-ultraviolet fluorooxoborates, *Sci. China Mater.*, 2020, **63**, 1480–1488.

44 M. Mutailipu, J. Han, Z. Li, F. M. Li, F. F. Zhang, X. F. Long, Z. H. Yang and S. L. Pan, Achieving the full-wavelength phase-matching for efficient nonlinear optical frequency conversion in $C(NH_2)_3BF_4$, *Nat. Photonics*, 2023, **17**, 694–701.

45 X. Wang, Y. Wang, B. B. Zhang, F. F. Zhang, Z. H. Yang and S. L. Pan, CsB_4O_6F: a congruent-melting deep-ultraviolet nonlinear optical material by combining superior functional units, *Angew. Chem., Int. Ed.*, 2017, **56**, 14119–14123.

46 Y. Wang, B. B. Zhang, Z. H. Yang and S. L. Pan, Cation-tuned synthesis of fluorooxoborates: towards optimal deep-ultraviolet nonlinear optical materials, *Angew. Chem., Int. Ed.*, 2018, **57**, 2150–2154.

47 M. Mutailipu, M. Zhang, H. P. Wu, Z. H. Yang, Y. H. Shen, J. L. Sun and S. L. Pan, $Ba_3Mg_3(BO_3)_3F_3$ polymorphs with reversible phase transition and high performances as ultraviolet nonlinear optical materials, *Nat. Commun.*, 2018, **9**, 3089.

48 J. Li, H. Li, G. Zhan and L. Zhang, Solar water splitting and nitrogen fixation with layered bismuth oxyhalides, *Acc. Chem. Res.*, 2017, **50**, 112–121.

49 M. Hu, C. C. Tu, Z. H. Yang, S. J. Han and S. L. Pan, $Sn_9O_4Br_9X$ (X = Cl, Br): Two new Sn(II) oxyhalides exhibiting large birefringence derived from highly distortive polyhedra of lone pair cations, *Scr. Mater.*, 2023, **231**, 115437.

50 L. Zhao, M. T. Fernandez-Diaz, L. H. Tjeng and A. C. Komarek, Oxyhalides: a new class of high-TC multiferroic materials, *Sci. Adv.*, 2016, **2**, 1600353–1600356.

51 Z. H. Yang, C. Hu, M. Mutailipu, Y. Z. Sun, K. Wu, M. Zhang and S. L. Pan, Oxyhalides: prospecting ore for optical functional materials with large laser damage thresholds, *J. Mater. Chem. C*, 2018, **6**, 2435–2442.

52 X. L. Chen and K. M. Ok, Metal oxyhalides: an emerging family of nonlinear optical materials, *Chem. Sci.*, 2022, **13**, 3942–3956.

53 H. Zhang, M. Zhang, S. Pan, X. Dong, Z. Yang, X. Hou, Z. Wang, K. B. Chang and K. R. Poeppelmeier, $Pb_{17}O_8Cl_{18}$: a promising ir nonlinear optical material with large laser damage threshold synthesized in an open system, *J. Am. Chem. Soc.*, 2015, **137**, 8360–8363.

54 Y. Huang, Z. Fang, B. Yang, X. Zhang and J. Mao, A new birefringent material, $HfF_2(IO_3)_2$, with a large birefringence and improved overall performances achieved by the integration of functional groups, *Scr. Mater.*, 2023, **223**, 115082.

55 C. Bai, B. L. Chen, K. W. Zhang, M. Zhang, S. L. Pan and J. J. Li, A new broad-band infrared window material $CdPbOCl_2$ with excellent comprehensive properties, *Dalton Trans.*, 2021, **50**, 16401–16405.

56 J. H. Jiao, A. Tudi, M. Zhang, W. B. Cai, J. J. Li, Z. H. Yang and S. L. Pan, Polymorphic $Pb_{14}O_8I_{12}$ and $Pb_7O_4I_6$ oxyhalides featuring unprecedented $[O_8Pb_{14}]$ clusters with broad IR transparency, *Sci. China Mater.*, 2022, **65**, 773–779.

57 C. Bai, Y. Chu, J. Z. Zhou, L. A. Wang, L. Luo, S. L. Pan and J. J. Li, Two new tellurite halides with cationic layers: syntheses, structures, and characterizations of $CdPb_2Te_3O_8Cl_2$ and $Cd_{13}Pb_8Te_{14}O_{42}Cl_{14}$, *Inorg. Chem. Front.*, 2022, **9**, 1023–1030.

58 J. Y. Guo, X. T. Zhan, J. T. Lan, X. Liu, S. Zhao, X. Xu, L. M. Wu and L. Chen, $Sb_4O_5I_2$: Enhancing Birefringence through Optimization of Sb/I Ratio for Alignment of Stereochemically Active Lone Pairs, *Inorg. Chem.*, 2024, **63**, 2217–2223.

59 L. Ma, W. Xu, L. Xu, Y. Lv, W. Liu, S. Guo and R. Tang, $CsSn_2(HPO_3)_2I$: The first inorganic metal phosphite iodide as a promising birefringent material exhibits a large birefringence with ideally layered framework, *Scr. Mater.*, 2024, **242**, 115913.

60 X. L. Chen, Q. Jing and K. M. Ok, $Pb_{18}O_8Cl_{15}I_5$: a polar lead mixed oxyhalide with unprecedented architecture and excellent infrared nonlinear optical properties, *Angew. Chem., Int. Ed.*, 2020, **59**, 20323–20327.

61 Z. X. Lu, F. F. Zhang, A. Tudi, Z. H. Yang, Z. Li and S. L. Pan, $Sn_{14}O_{11}Br_6$: a promising birefringent material with a $[Sn_{14}O_{11}Br_6]$ layer, *J. Mater. Chem. C*, 2021, **9**, 7103–7109.

62 S. J. Han, A. Tudi, W. B. Zhang, X. L. Hou, Z. H. Yang and S. L. Pan, Recent development of SnII, SbIII-based birefringent material: crystal chemistry and investigation of birefringence, *Angew. Chem., Int. Ed.*, 2023, **62**, e202302025.

63 Y. Xu, C. Lin, D. Zhao, B. Li, L. Cao, N. Ye and M. Luo, Chemical substitution–oriented design of a new polar $PbFIO_3$ achieving a balance between large second-harmonic generation response and wide band gap, *Scr. Mater.*, 2022, **208**, 114347.

64 C. H. Hu, X. T. Cai, M. F. Wu, Z. H. Yang, J. Han and S. L. Pan, Lone pair-driven enhancement of birefringence in polar alkali metal antimony phosphates, *Chem. Mater.*, 2022, **34**, 4224–4231.

65 Y. Xiao, M. M. Chen, Y. Y. Shen, P. F. Liu, H. Lin and Y. Liu, $A_3Mn_2Sb_3S_8$ (A = K and Rb): a new type of multifunctional infrared nonlinear optical material based on unique three-dimensional open frameworks, *Inorg. Chem. Front.*, 2021, **8**, 2835–2843.

66 C. Liu, S. H. Zhou, C. Zhang, Y. Y. Shen, X. Y. Liu, H. Lin and Y. Liu, $CsCu_3SbS_4$: rational design of a two-dimensional layered material with giant birefringence derived from Cu_3SbS_4, *Inorg. Chem. Front.*, 2022, **9**, 478–484.

67 C. Liu, S. H. Zhou, Y. Xiao, C. Zhang, H. Lin and Y. Liu, Aliovalent-cation-substitution-induced structure transformation: a new path toward high-performance IR nonlinear optical materials, *J. Mater. Chem. C*, 2021, **9**, 15407–15414.

68 C. H. Hu, M. F. Wu, J. Han, Z. H. Yang, S. J. Han and S. L. Pan, New antimony fluorooxoborates with strong birefringence and unprecedented structural characterisation, *Chem. Commun.*, 2024, **60**, 2653–2656.

69 V. Jo, M. K. Kim, D. W. Lee, I. W. Shim and K. M. Ok, Lone pairs as chemical scissors in new antimony oxychlorides, $Sb_2ZnO_3Cl_2$ and $Sb_{16}Cd_8O_{25}Cl_{14}$, *Inorg. Chem.*, 2010, **49**, 2990–2995.

70 A. Abudurusuli, J. Li and S. Pan, A review on the recently developed promising infrared nonlinear optical materials, *Dalton Trans.*, 2021, **50**, 3155–3160.

71 H. Katzke, Y. Oka, Y. Kanke, K. Kato and T. Yao, Structure of triantimony tetraoxide chloride, Sb_3O_4Cl: twinning and one-dimensional disorder, *Cryst. Mater.*, 1999, **214**, 284–289.

72 Z. Hugonin, M. Johnsson and S. Lidin, Two for the price of one resolvable polymorphism in a single crystal of alpha- and beta-Sb_3O_4I, *Solid State Sci.*, 2009, **11**, 24–28.

73 P. Patnaik, *Handbook of Inorganic Compounds*, McGraw-Hill Pub. Co., Toronto, 2003, pp. 55–56.

74 L. D. Freedman, G. O. D1oak, G. G. Long, T. Mahmood and C. B. Lindhal, *Kirk-Othmer Encyclopedia of Chemical Technology*, John Wiley & Sons, Inc., Toronto, 2003, Section 2.7, pp. 56–87.

75 X. Su, Y. Liu, C. Xiao, G. Zhang, T. Liu, J. Qin and C. Chen, A facile, clean and quantitative synthesis of antimony chloride oxide single crystals, *Mater. Lett.*, 2006, **60**, 3879–3881.

76 S. Menchetti, C. Sabelli and R. Trosti-Ferronj, The structures of onoratoite, $Sb_8O_{11}Cl_2$ and $Sb_8O_{11}Cl_2.6H_2O$, *Acta Crystallogr., Sect. C: Cryst. Struct. Commun.*, 1984, **40**, 1506–1510.

77 Z. Mayeroa, M. Johnsson and S. Lidin, The structure of onoratoite, $Sb_8O_{11}X_2$ (X = Cl, Br) revisited, *Solid State Sci.*, 2006, **8**, 849–854.

78 H. P. Wu, S. L. Pan, K. R. Poeppelmeier, H. Y. Li, D. Z. Jia, Z. H. Chen, X. Y. Fan, Y. Yang, J. M. Rondinelli and H. S. Luo, $K_3B_6O_{10}Cl$: A new structure analogous to perovskite with a large second harmonic generation response and deep UV absorption edge, *J. Am. Chem. Soc.*, 2011, **133**, 7786–7790.

79 M. Xia, B. Xu, L. Liu, X. Wang, R. Li and C. Chen, Thermophysical properties of nonlinear optical crystal $K_3B_6O_{10}Br$, *J. Appl. Crystallogr.*, 2016, **49**, 539–543.

80 H. Qiu, F. Li, Z. Li, Z. Yang, S. Pan and M. Mutailipu, Breaking the inherent interarrangement of $[B_3O_6]$ clusters for nonlinear optics with orbital hybridization enhancement, *J. Am. Chem. Soc.*, 2023, **145**, 24401–24407.

81 M. Zhang, S. L. Pan, X. Y. Fan, Z. X. Zhou, K. R. Poeppelmeier and Y. Yang, Crystal growth and optical properties of a noncentrosymmetric haloid borate, $K_3B_6O_{10}Br$, *CrystEngComm*, 2011, **13**, 2899.

82 B. B. Zhang, M. H. Lee, Z. H. Yang, Q. Jing, S. L. Pan, M. Zhang, H. P. Wu, X. Su and C. S. Li, Simulated pressure-induced blue-shift of phase-matching region and nonlinear optical mechanism for $K_3B_6O_{10}X$ (X = Cl, Br), *Appl. Phys. Lett.*, 2015, **106**, 031906.

83 M. Hu, N. Tuerhong, Z. H. Chen, Q. Jing and M. H. Lee, $Li_3B_8O_{13}X$ (X = Cl and Br): two new noncentrosymmetric crystals with large birefringence induced by BO_3 units, *Inorg. Chem.*, 2023, **62**, 3609–3615.

84 P. Yu, L. M. Wu, L. J. Zhou and L. Chen, Deep-ultraviolet nonlinear optical crystals: $Ba_3P_3O_{10}X$ (X = Cl, Br), *J. Am. Chem. Soc.*, 2014, **136**, 480–487.

85 G. H. Zou, C. S. Lin, H. Jo, G. Nam, T. S. You and K. M. Ok, Pb_2BO_3Cl: A tailor-made polar lead borate chloride with very strong second harmonic generation, *Angew. Chem., Int. Ed.*, 2016, **55**, 12078–12082.

86 M. Luo, Y. X. Song, F. Liang, N. Ye and Z. S. Lin, Pb_2BO_3Br: A novel nonlinear optical lead borate bromine with a KBBF-type structure exhibiting strong nonlinear optical response, *Inorg. Chem. Front.*, 2018, **5**, 916–921.

87 H. W. Yu, N. Z. Koocher, J. M. Rondinelli and P. S. Halasyamani, Pb_2BO_3I: A borate iodide with the largest second-harmonic generation (SHG) response in the $KBe_2BO_3F_2$ (KBBF) family of nonlinear optical (NLO) materials, *Angew. Chem., Int. Ed.*, 2018, **57**, 6100–6103.

88 T. Zheng, Q. Wang, J. X. Ren, L. L. Cao, L. Huang, D. J. Gao, J. Bi and G. H. Zou, Halogen regulation triggers structural transformation from centrosymmetric to noncentrosymmetric switches in tin phosphate halides Sn_2PO_4X (X= F, Cl), *Inorg. Chem. Front.*, 2022, **9**, 4705–4713.

89 J. Y. Guo, A. Tudi, S. J. Han, Z. H. Yang and S. L. Pan, Sn_2PO_4I: An excellent birefringent material with giant optical anisotropy in non-π-conjugated phosphate, *Angew. Chem., Int. Ed.*, 2021, **60**, 24901–24904.

90 J. Y. Guo, A. Tudi, S. J. Han, Z. H. Yang and S. L. Pan, $Sn_2B_5O_9Cl$: A material with large birefringence enhancement activated prepared via alkaline-earth-metal substitution by tin, *Angew. Chem., Int. Ed.*, 2019, **58**, 17675–17678.

91 J. Y. Guo, S. C. Cheng, S. J. Han, Z. H. Yang and S. L. Pan, $Sn_2B_5O_9Br$ as an outstanding bifunctional material with strong second-harmonic generation effect and large birefringence, *Adv. Opt. Mater.*, 2021, **9**, 2001734.

92 X. Li, C. Hu, F. Kong and J. Mao, Structure and optical property evolutions in $PbM(PO_4)X$ (M = Zn, Sn; X = halogen): SHG effect and birefringence, *Inorg. Chem. Front.*, 2023, **10**, 2268.

93 J. Y. Guo, A. Tudi, X. Q. Lu and S. J. Han, Noncentrosymmetric versus centrosymmetric: halogen induced variable coordination modes of Sn^{2+} and structural transition in $Sn_3B_3O_7X$ (X = Cl and Br), *Inorg. Chem.*, 2023, **62**, 679–684.

94 J. H. Jiao, M. Cheng, R. Yang, Y. C. Yan, M. Zhang, F. F. Zhang, Z. H. Yang and S. L. Pan, Promising deep-ultraviolet birefringent materials via rational design and assembly of planar π-conjugated $[B(OH)_3]$ and $[B_3O_3(OH)_3]$ functional species, *Angew. Chem., Int. Ed.*, 2022, **61**, e202205060.

